

Journal of Biomedical Optics

SPIEDigitalLibrary.org/jbo

Innovative optical microsystem for static and dynamic tissue diagnosis in minimally invasive surgical operations

Roozbeh Ahmadi
Muthukumaran Packirisamy
Javad Dargahi

Innovative optical microsystem for static and dynamic tissue diagnosis in minimally invasive surgical operations

Roozbeh Ahmadi, Muthukumaran Packirisamy, and Javad Dargahi

Concordia University, Optical Bio Micro-systems Lab, Tactile Sensing and Medical Robotics Lab, Department of Mechanical and Industrial Engineering, Montreal, Quebec H3G 2W1, Canada

Abstract. During conventional surgical tasks, surgeons use their tactile perception in their finger tips to sense the degree of softness of biological tissues to identify tissue types and to feel for any abnormalities. However, in robotic-assisted surgical systems, surgeons are unable to sense this information because only surgical tools interact with tissues. In order to provide surgeons with such useful tactile perception, therefore, a tactile sensor is required that is capable of simultaneously measuring contact force and resulting tissue deformation. Accordingly, this paper discusses the design, prototyping, testing, and validation of an innovative tactile sensor that is capable of measuring the degree of softness of soft objects such as tissues under both static and dynamic loading conditions and which is also magnetic resonance compatible and electrically passive. These unique characteristics of the proposed sensor would also make it a practical choice for use in robotic-assisted surgical platforms. The prototype version of this sensor was developed by using optical micro-systems technology and, thus far, experimental test results performed on the prototyped sensor have validated its ability to measure the relative softness of artificial tissues. © 2012 Society of Photo-Optical Instrumentation Engineers (SPIE). [DOI: [10.1117/1.JBO.17.8.081416](https://doi.org/10.1117/1.JBO.17.8.081416)]

Keywords: optical microsystems; optical fiber; tactile sensor; tissue diagnosis; minimally invasive robotic surgery.

Paper 11755SS received Dec. 14, 2011; revised manuscript received Jun. 4, 2012; accepted for publication Jul. 3, 2012; published online Aug. 8, 2012.

1 Introduction

In recent years, the use of advanced diagnostic medical devices in surgical tasks has increased at a fast pace. Such surgical tasks range from conventional minimally invasive surgery (MIS) to sophisticated minimally invasive robotic surgery (MIRS) and catheter-based cardiovascular techniques (CBT). In fact, the success of robotic-assisted surgical platforms, such as the daVinci surgical system (Intuitive Surgical Inc.),¹ has demonstrated the advantages of such platforms over traditional open-surgery techniques. Also the Amadeus Surgical Robot,^{2,3} has been developed by the Titan Medical, Inc., Canada although this system has not yet been made commercially available. It offers enhanced features such as improved vision systems, long-distance tele-surgical applications, and force feedback. Although Amadeus offers a force feedback feature, it does not provide tactile feedback. Similarly, robotic catheter systems such as the Sensai Robotic Navigation System,⁴ developed by the Hansen Medical Inc., provides surgeons only with force feedback and not with tactile feedback whenever the tip of the catheters interacts with vessel walls or cardiac tissues. In brief, despite the advantages of such systems, they still suffer from a number of inadequacies. The lack of reliable tactile sensors capable of measuring tactile information between surgical tools and tissues is one of the main causes of such inadequacy.^{5,6} In order to respond to this shortcoming, tactile sensors are needed to mimic the palpation performed by surgeon's fingertips. Such tactile sensors would provide the necessary sensory feedback⁷ that would enable surgeons to characterize and

diagnose abnormal tissue areas (tumorous lumps),⁸ blood vessels (arteries and veins),⁹ and ureters. As a result, the development of a tactile sensor that replicates the perception of the surgeon's fingertips is crucial for diagnosing purposes in minimally invasive surgical systems. During tool-tissue interactions, such a tactile sensor would measure the relative softness of the contact tissue and the local discontinuities in the softness. Technically, the degree of softness can be measured using various methods. In the present study, Shore (Durometer) type A and type OO scales are used to measure the softness of tested artificial tissues. The softness of a material is dependent on mechanical properties such as its stiffness and modulus of elasticity.

The softness of a tissue is sensed by the tactile sensor in a similar manner to the surgeon's fingertip whereby the less hard the material actually is, the softer it feels. Similar to the surgeons' fingertips, the tactile sensor will diagnose the tissue based on its type and degree of softness. The term "softness" is used for characterizing soft objects while the term "hardness" is mainly reserved for hard objects.

To develop a tactile sensor for surgical diagnosis, four design constraints are taken into consideration. First, there is the need to ensure that the sensor is immune from the effects of magnetic flux and radiation since surgical procedures, in the presence of magnetic resonance imaging (MRI) devices, are likely to become more commonplace in the future.¹⁰⁻¹² Second, for safety concerns, it is necessary to ensure that no electric current permeates from the sensor into the patient's body. For example, in intracardiac surgeries, introducing electrical currents might result in disturbing the normal electrical activities in the heart.¹³ Third, surgeons usually need to feel tactile information while, at the same time,

Address all correspondence to: Muthukumaran Packirisamy, Concordia University, Optical Bio Micro-systems Lab, Tactile Sensing and Medical Robotics Lab, Department of Mechanical and Industrial Engineering, Montreal, Quebec H3G 2W1, Canada. Tel: (514) 848-2424 ext. 7973; E-mail: pmuthu@alcor.concordia.ca

maintaining a stable contact between robotic surgical tools (e.g., graspers or catheter-tips) and tissues. During such stable contact, the tool-tissue interaction force is in static loading condition. Fourth, only a very small space is available at the tips of surgical tools for the integration of tactile sensors. As a result of these four constraints, the tactile sensor ideally should be MRI-compatible, electrically passive, capable of performing under combined static and dynamic loading conditions, and miniaturized.

Recently, numerous tactile sensors have been proposed for use in surgical tasks¹⁴⁻¹⁶ among which are those based on electrical sensing principles such as strain gauges,¹⁷ piezoelectric,^{18,19} piezoresistive,^{20,21} and capacitive.¹⁴ All these, however, are neither MRI-compatible nor electrically passive. Moreover, such electrical-based sensors, especially those which are piezoelectric-based,¹⁸ cannot perform optimally under static loading conditions. Considering the size constraints, optical microsystems are one of the few choices that can address all the above-mentioned design constraints.²² Although a number of MRI-compatible optical sensors²²⁻²⁶ have been proposed for use in surgical tasks, they only measure force and not tissue softness.

In previous work undertaken by the authors,²⁷ a novel optical-based

tactile sensor was introduced which is both MRI-compatible and electrically passive but was neither capable of measuring the degree of softness of tissue nor was it miniaturized. Recently, however, we have designed an optical-based tactile sensor that has overcome these two missing criteria and it is the purpose of this paper to describe its fabrication and testing. Being optically-based, it is safe to use this sensor in MIS, MIRS, and CBT procedures in order to measure the relative softness of soft objects such as biological tissues. Furthermore, test results of the tests confirm that the sensor is able to distinguish between three artificial tissues with different degrees of softness as is found in actual biological tissues in real surgical situations. In addition, in contrast to existing sensors, the tactile sensor proposed in this study is MRI-compatible, electrically passive, and able to perform under both static and dynamic loading conditions.

2 Sensor Design

Figure 1 illustrates the structural design of the proposed sensor to measure the relative softness of objects such as biological tissues. The sensor is able to measure both the contact force and the resulting deformation of soft objects. As a result, the sensor has two layers of sensing elements in which one layer measures the contact force, while the other measures the tissue deformation.

The sensor consists of nine silicon structural parts, three elastomeric foundations, and three pairs of optical fibers. The nine silicon parts from N-Type <100> silicon wafer include one substrate, three chips micro-machined with v-grooves, four supports, and one beam micro-machined with v-grooves. The elastic foundations are made from polydimethylsiloxane (PDMS) polymer material. The optical fibers used in this design are single-mode fibers.

As can be seen in Figure 1, the elastic foundations are mounted on the substrate, and three chips with v-grooves are mounted on the elastic foundations. Two pairs of optical fibers (Fibers B Left/Right and C Left/Right) are integrated into the v-grooves of the chips. The integrated Fibers B and C measure the relative displacement of the elastic foundations at the left and right ends, respectively, for estimating the contact force. The

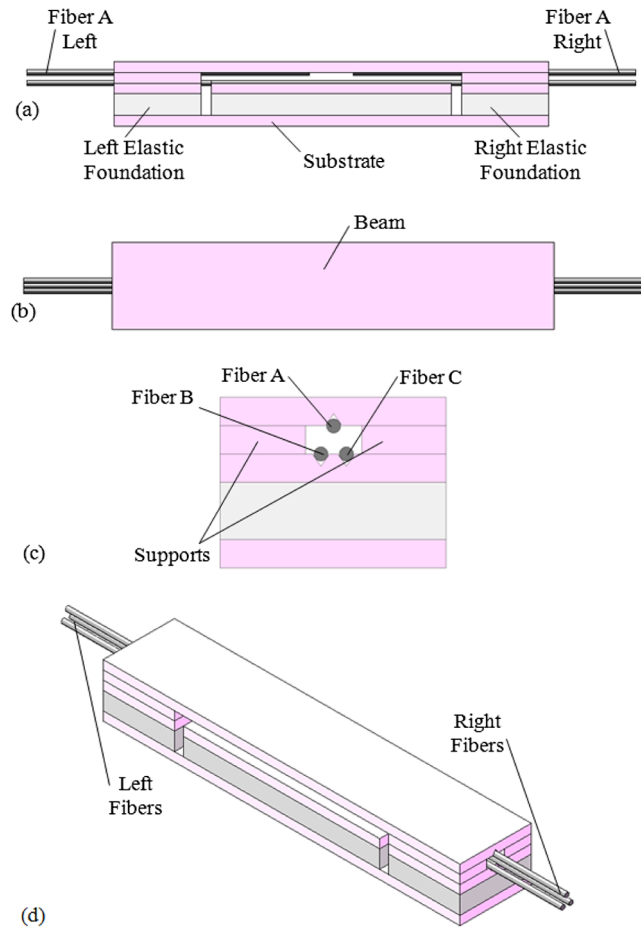


Fig. 1 The structural design of the sensor: (a) front view; (b) top view; (c) side view; and (d) 3-D view.

beam with v-grooves is fixed on the end supports so the beam is assumed to have fixed-fixed boundary conditions in bending. A pair of optical fibers (Fibers A Left/Right) is integrated into the v-groove of the beam to measure the deformation of soft objects for estimating the relative softness.

The arrangement of optical fibers inside the v-grooves of the supports, and the beam is shown in Fig. 2. This figure presents the top view of the sensor in which the beam is cross-sectioned in order that the arrangement of the fibers can be clearly visualized. Fiber A Left and Fiber A Right are integrated into the v-groove micro-machined on the bottom surface of the beam as shown in Fig. 2 in such a way that there is a gap between the bare ends of Fiber A Left and Fiber A Right in the mid-region of the beam.

Fiber B Left is integrated into the v-groove of the left support chip and is terminated at the edge of the chip, while Fiber B Right is integrated into the v-grooves of the right support chip and middle chip and is terminated at the left edge of the middle chip as shown in Fig. 2. Fiber C Left is integrated into the v-grooves of the left support chip and middle chip and is terminated at the right edge of the middle chip as shown in Fig. 2. Similarly, Fiber C Right is integrated into the v-groove of the right support chip and is terminated at the left edge of this chip. In order to facilitate relative displacements between the end and the middle supports, small gaps are provided between the left and the right parts of Fiber B and Fiber C.

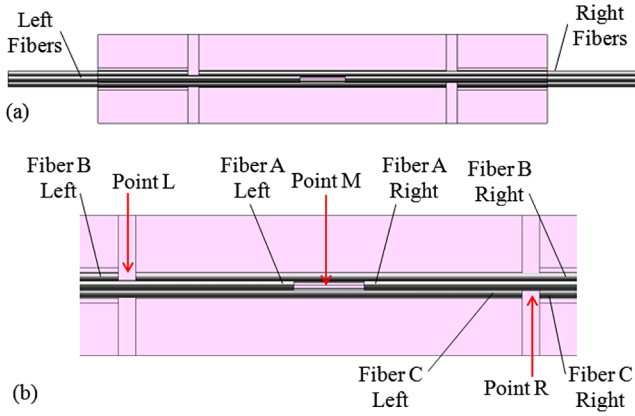


Fig. 2 The configuration of the optical fibers on the silicon parts of the sensor: (a) the top view in which the sensor beam is transparent for better visualization; and (b) the magnified version of the top view.

In order to measure the relative softness of the tissue to be contacted (Fig. 3), the amplitude of the interacting load between the sensor and the tissue as well as the resultant deformation of the tissue itself, must be measured simultaneously. In the proposed design, the deformation of soft objects is measured by Fiber A through bending of the beam, while Fibers B and C measure the contact force at the left and right ends, respectively.

The load applied to the sensor results in the compression of the left and right elastic foundations (PDMS layers in this case) of the sensor. As a result, an optical misalignment occurs between the Fiber B Left and the Fiber B Right at point (l) on the left side of the sensor, as shown in Fig. 3. Similarly, on the right side, an optical misalignment occurs between the Fiber C Left and the Fiber C Right at point (r), as shown in Fig. 3. By measuring the loss in optical transmission due to misalignment through Fiber B at point (l) and through Fiber C at point (r), the amplitude of the load can be measured. Similarly, the angular deflection of the beam at its central point can be determined by measuring the coupling loss between Fiber A Left and Fiber A Right at point (m), as shown in Fig. 3, and which represents the resultant deformation of the contact tissue. As shown in Fig. 4, hard objects result in small deflection of the beam, while soft objects result in a large deflection for the same amount of force as measured by Fibers B and C. To summarize, the higher the softness of the contact object, the larger the deflection of the beam and the greater the angular misalignment between Fiber A-left and Fiber A-Right. This deflection indicates the degree of softness, which is an important parameter when characterizing biological tissues during MIS, MIRS, and CBT procedures.

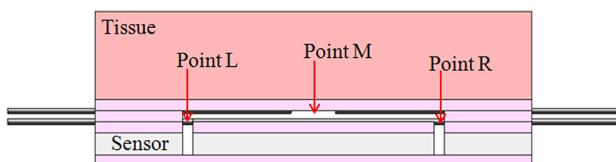


Fig. 3 The sensor is contacting a soft object to measure the degree of softness.

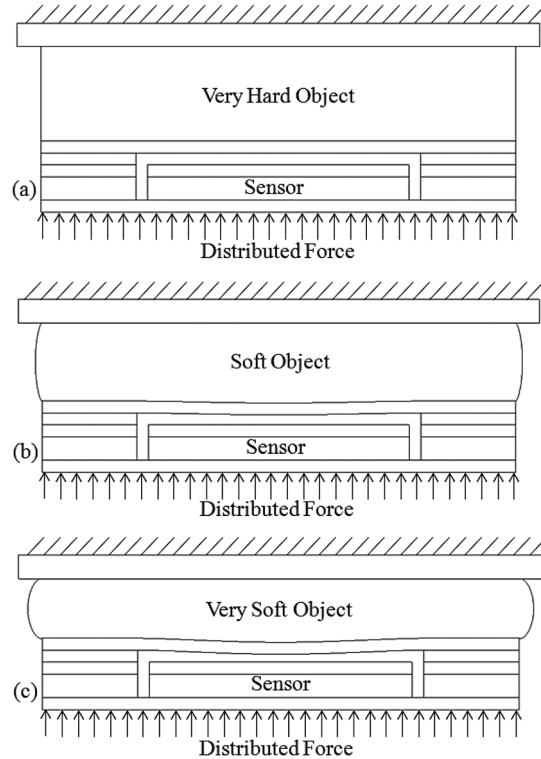


Fig. 4 For the same amount of distributed force applied to the tissue by the sensor, the greater the object's degree of softness, the greater the deflection of the sensor beam. In (a), the object is very hard. The object in (b) is harder than that in (c).

3 Sensor Modeling

When the sensor interacts with a soft object, it measures the contact force as well as the resulting deformation of the soft object. The contact force is measured by Fibers B and C, whereas the resulting deformation is measured by Fiber A. The sensing principle relies on measuring the coupling loss between each pair of fibers. For the force measurement, the contact force results in a lateral misalignment between each pair of fibers which results in coupling loss. However, for the deformation measurement, the deformation of the contact object results in the deflection of the sensor beam, and the deflection results in the angular misalignment between the pairs of Fiber A with resultant coupling loss. The theoretical considerations involved with the force measurement and the deformation measurement are slightly different.

3.1 Force Measurement

The coupling loss (dB) due to the lateral misalignment between Fiber B Left and Fiber B Right is modeled theoretically as is the relation between the contact force, the resulting lateral misalignment, and the sensor output. Based on that, the theoretical explanation of the relationship between the contact force and the sensor output is investigated.

The coupling efficiency caused by the misalignment of Fiber A Left and Fiber A Right of the sensor can be defined as η_{Force} .^{28,29}

$$\eta_{Force} = 4 \frac{D}{B} \exp \left[-A \frac{C}{B} \right], \quad (1)$$

where

$$A = \frac{(kw_{BL})^2}{2} \quad (2)$$

$$B = G^2 + (D + 1)^2 \quad (3)$$

$$C = (D + 1)F^2 \quad (4)$$

$$D = \left(\frac{w_{BR}}{w_{BL}}\right)^2 \quad (5)$$

$$G = 2\frac{Q}{kw_{BL}^2} \quad (6)$$

$$F = 2\frac{\Delta\ell}{kw_{BL}^2}, \quad (7)$$

in which k is the propagation constant of the gap media between fibers. w_{BL} and w_{BR} are the Gaussian mode field radius of Fiber A Left and Fiber A Right, respectively. Q is the gap between Fiber A Left and Fiber A Right and $\Delta\ell$ is the lateral displacement between the axis of Fiber A Left and Fiber A Right.

$$k = \frac{2\pi n_0}{\lambda} \quad (8)$$

$$w_{BL} = a\left(0.65 + \frac{1.619}{V^{3/2}} + \frac{2.879}{V^6}\right) \quad (9)$$

$$w_{BR} = w_{BL} \quad (10)$$

$$V = \frac{2\pi a}{\lambda} \sqrt{n_{\text{core}}^2 - n_{\text{cladding}}^2}, \quad (11)$$

in which n_0 , n_{core} , and n_{cladding} are the refractive indices of the media, of the core of fibers, and of the cladding of fibers, respectively; a is the radius of the core of the fiber and λ is the wavelength of the light. Δl is derived due to the linear elastic behavior of the elastic foundation.³⁰ In fact, the PDMS is modeled as a linear elastic material since the deformations applied to the elastic foundation are small in this case.

$$\Delta l = \frac{l}{EA}F, \quad (12)$$

where l is the initial thickness of the PDMS layer; E is the modulus of elasticity of the PDMS; A is the area of the small chip, which is mounted on the small PDMS layer; and F is the contact force. Now, based on the coupling efficiency and the power of the light source (P_{BL}), the power of the coupled light from Fiber B Left into Fiber B Right (P_{BR}) can be obtained as:

$$P_{BR} = \eta_{\text{Force}}P_{BL}, \quad (13)$$

which converts the light intensity of Fiber B Right into the electric voltage, V_{BR} . Consequently, the electric output voltage of the sensor is the electric voltage, which is linearly proportional to P_{BR} which means that the sensor output voltage can be calculated as follows:

$$V_{BR} = R(\lambda, \text{LOAD})P_{BR}, \quad (14)$$

in which $R(\lambda, \text{LOAD})$ is the multiplication of the spectral responsiveness of the photodetector and the resistance of an external load. The spectral responsiveness, which is a function of the light wavelength, can be obtained from the specifications of the photodetector. The external load resistance, which defines the sensitivity of the voltage measurement, can be tuned. Ultimately, using a DAQ, the output voltage can be readily observed using LabVIEW software. Such theoretical formulations provide the contact force on the left side of the sensor. The same theory is applied between Fiber C Left and Fiber C Right so as to model the contact force applied on the right side of the sensor.

3.2 Deformation Measurement

The coupling loss (dB) due to the angular misalignment between optical Fiber A Left and optical Fiber A Right of the sensor is proportional to the deformation of the contacted soft object. As previously stated, for the same amount of contact force, the greater the tissue softness and beam deflection with consequent increase in angular misalignment between Fiber A Left and Fiber A Right. Here the relation between the angular misalignment and the sensor output is modeled. The coupling efficiency caused by the misalignment between Fiber A Left and Fiber A Right of the sensor can be defined as $\eta_{\text{Deformation}}$ which is derived from Eqs. (1) to (11) where BL and BR subscripts are changed to AL and AR subscripts, respectively by using Eq. (15) instead of Eq. (4):^{28,29}

$$C = D(G^2 + D + 1)\sin^2(\Delta\theta). \quad (15)$$

w_{AL} and w_{AR} are the Gaussian mode-field radius of Fiber A Left and Fiber A Right, respectively; Q is the gap between Fiber A Left and Fiber A Right and $\Delta\theta$ is the angular misalignment between the axis of Fiber A Left and Fiber A Right.

Now, based on the coupling efficiency and the power of the light source, P_{AL} , the power of the coupling light into Fiber A Right, the P_{AR} , can be obtained as follows:

$$P_{AR} = \eta_{\text{Deformation}}P_{AL}. \quad (16)$$

Fiber A Right is coupled to a sensor containing a photodetector which converts the light intensity of the fiber into an electric voltage, V_{AR} . Consequently, the output of the sensor is the electric voltage, which is linearly proportional to P_{AL} and can be determined using Eq. (14) as described in Sec. 3.1. Similar to the sensor output from Fibers B and C, the output voltage for Fiber A (V_{AR}) is recorded on LabVIEW. $\Delta\theta$ increases and V_{AR} becomes lower in proportion to the softness of the contact object.

In the present although this paper presents the conceptual aspect of a current mathematical model of a sensor that is capable measuring relative softness it can also be used as a basis for the quantitative measurement of material properties of tissues for any future work.

4 Sensor Prototyping

4.1 Sensor Micro-Fabrication

An illustration of the sensor components are shown in Fig. 5. The substrate (Layer A) and the four supports (Layer D) of the sensor were diced precisely from an N-Type <100> silicon wafer. The elastic foundations (Layer B) were made of PDMS films. A Sylgard 184 silicone elastomer kit (Dow Corning Co., MI) with the ratio of 10:1 was used to make the PDMS films. The thickness of this layer was 500 μm . In order to achieve a uniform layer with a smooth surface quality, a spin coater was used to coat the PDMS layer on a silicon wafer. The layers were then diced into small strips with the required dimensions. Another N-Type <100> silicon wafer was used to make the v-grooved parts of the sensor (Layer A and Layer E). An anisotropic wet-etching with buffered hydrofluoric acid (BHF) and tetramethylammonium hydroxide (TMAH) was used to micro-machine the v-grooves on the silicon wafer after which a wafer-dicing machine was used to cut out the chips and the beam from the micro-machined silicon wafer.

4.2 Sensor Assembly

After the micro-machining of the sensor components, they are assembled. First, the v-grooved chips were placed on the elastic foundations [Fig. 5(b)] and mounted on the substrate. Afterward, the optical fibers were placed and glued appropriately inside the v-grooves of the chips upon which the supports were fixed on the chips. The fibers were then integrated into the middle v-groove of the beam. Finally, the beam was accordingly placed and fixed on the supports.

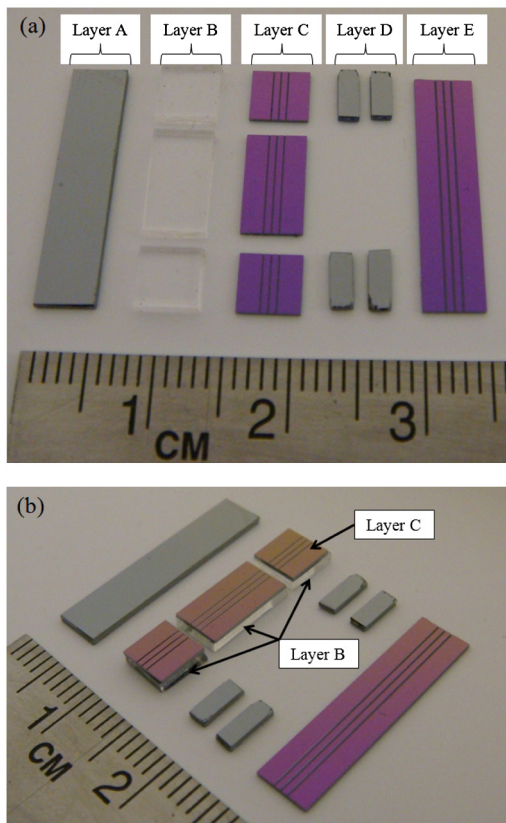


Fig. 5 The components of the sensor before assembly.

Scanning electron-microscopy (SEM) imaging techniques were applied to examine the size and the surface quality of the v-grooves and also to evaluate how accurately the fibers were integrated into the v-grooves. Figure 6(a) illustrates the SEM images of the micro-machined v-grooves at the edge of the middle chip with only one fiber integrated into the chip. The adjacent v-groove was intentionally left empty to visualize the cross section of the micro-machined v-groove. Figure 6(b) illustrates the terminated end of the fiber at the edge of the middle chip.

5 Experimental Setup

Softness measurement of artificial tissues and also for the measurement of local discontinuities in the softness of these tissues. Figure 7 illustrates the experimental setup. The light source is connected to Fibers A Left, B Left, and C Left. Fibers A Right, B Right, and C Right are connected to three photodetectors. The light source is an HP-371 superluminescent diode (SLD) from Superlum (Ireland). At the full-width-half-maximum (FWHM) of the SLD, its spectral bandwidth and center wavelength are 53 and 843 nm, respectively. The photodetectors are DET02AFC with the wavelength range of 400 to 1100 nm, from Thorlabs (NJ). Using a DAQ (an NI PCI-6225 from National Instruments), the electrical output signals of the photodetectors are digitized and stored in the connected computer. Using an ElectroForce 3200 test instrument from Bose (MN), the sensor was tested experimentally. The test instrument comes with a software interface called WinTest which provides

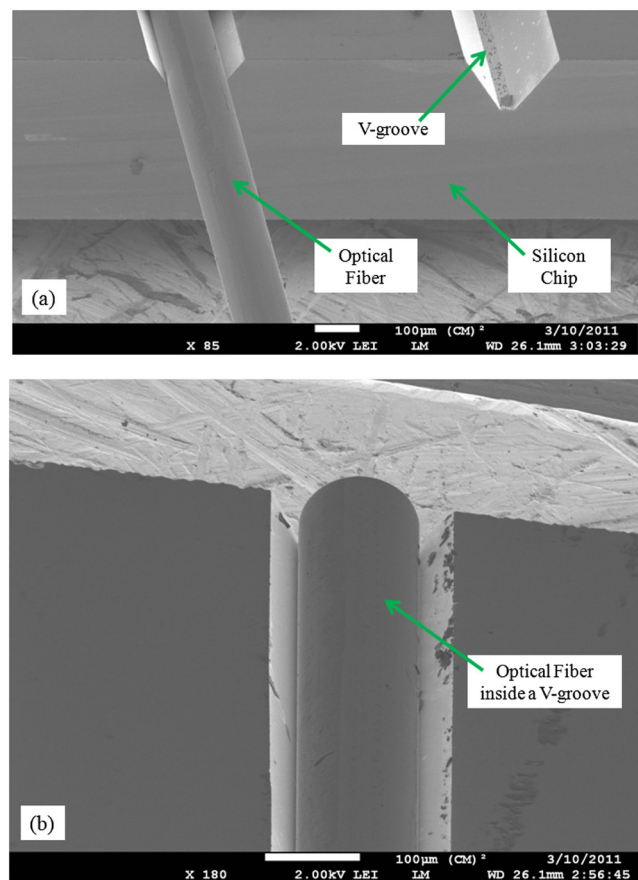


Fig. 6 The SEM images of the optical fibers integrated into the v-grooves.

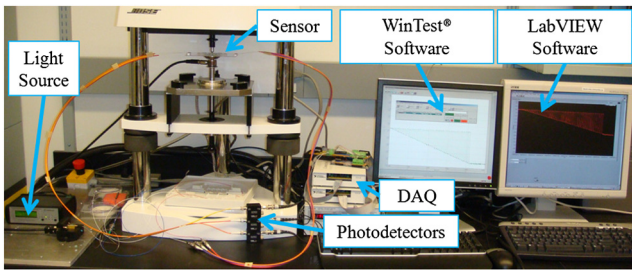


Fig. 7 The photograph of the experimental setup.

a user-friendly environment to control the test parameters such as force and displacement. Known reference force/displacement functions, customized on the WinTest software, were applied to the test setup. The output voltage of the photodetectors was measured on the LabVIEW software.

Figure 8 shows the sensor under experimental tests. A number of test setup scenarios were used. The sensor was placed on the low jaw of the Bose test instrument. In the first scenario, the sensor was tested under a concentrated force applied to the sensor beam, whereas in the second scenario, the sensor was tested while interacting with artificial tissues. The first scenario was chosen to examine the response of the sensor under static loading conditions. The second scenario was set up to validate

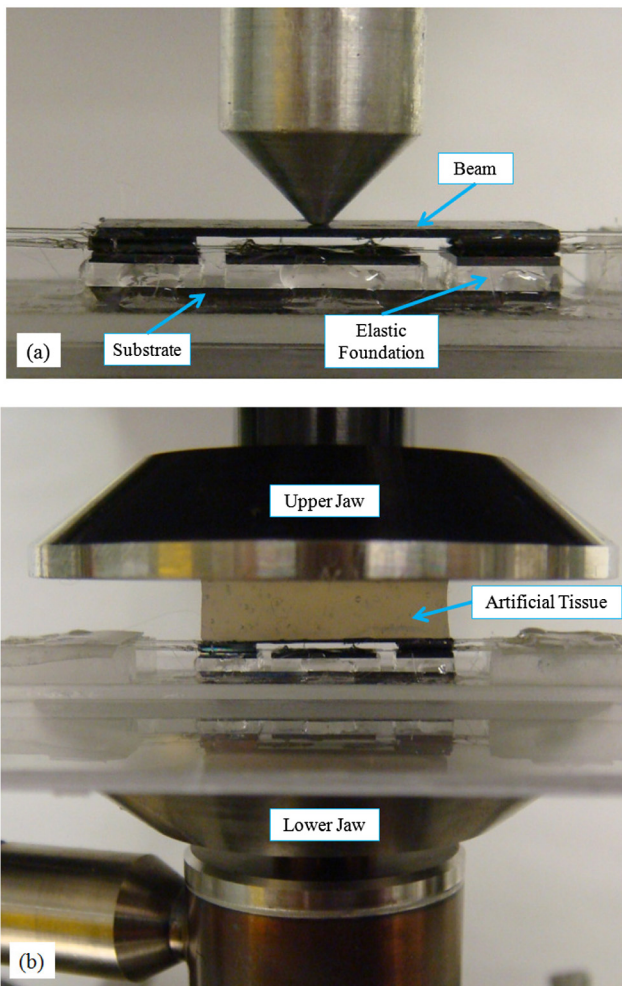


Fig. 8 The photograph of the sensor under the experimental tests: (a) test with concentrated force; and (b) test with distributed force.

the sensor ability to measure the relative softness. In Fig. 8(a), the sensor was tested with concentrated forces applied from an indenter to different points on the sensor beam. Figure 8(b) shows the sensor measuring the softness of an artificial tissue.

6 Tests Results and Discussion

To evaluate the performance of the sensor in measuring the relative softness of tissues, the sensor was tested with three artificial tissues with different degrees of softness. Figure 9 shows the output of the sensor while contacting the artificial tissues. In this test, the setup is the same as the test configuration shown in Fig. 8(b). Three silicone rubber materials with different degrees of softness were used as artificial tissues. In the previous work presented by the authors,^{20,21} it was shown that the silicone rubbers have similar material properties to biological tissues. The following silicone rubber materials were used: 1) the 10-OO with the degree of softness equal to 10 Shore on scale OO; 2) the 30-OO with the degree of softness equal to 30 Shore on scale OO; and 3) the 20-A with the degree of softness equal to 20 Shore on scale A. Among these three materials, 10-OO is the softest material, whereas 20-A is the hardest. A triangle function was chosen to examine the linearity and hysteresis of sensor outputs. For the frequency of force function, the relatively slow rate of 0.1 Hz was chosen to observe any potential relaxation of the artificial tissues. During the tests, the lower jaw was fixed and a force, in the form of a triangular waveform, was applied from the upper jaw. This condition was repeated for all three silicone rubber materials.

As shown in Fig. 9, Fibers B and C measure the force, while Fiber A measures the degree of softness of the contact objects. For the three tested materials, Fibers B and C measure the same force. However, the output of Fiber A varies in the three tested materials. The more the voltage drops for Fiber A, the softer the material. Using this concept, the results show that the 10-OO is softer than the 30-OO and 20-A is hardest. This comparison confirms the capability of the sensor to measure the softness of soft contact objects in a relative way. These artificial tissues can represent three biological tissues in real surgical conditions. As an example, they can represent mitral valve leaflet tissue (softest), left atrium tissue (medium), and mitral valve annulus tissue (hardest) in cardiovascular mitral valve repair surgery. Among them, the leaflet is the softest one, the

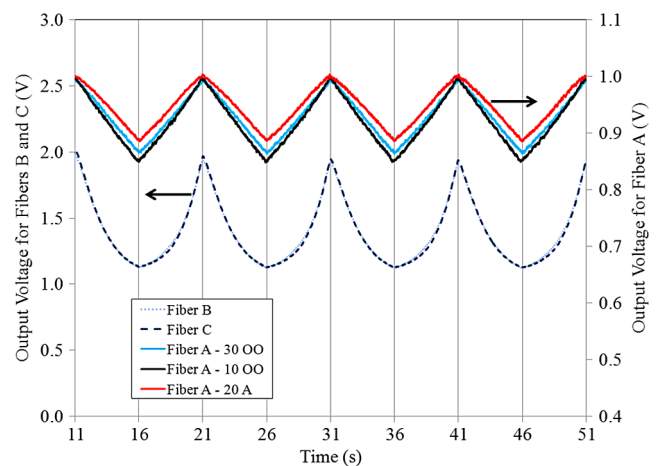


Fig. 9 The output of the sensor during the interaction with three artificial tissues with different degrees of softness. The sensor distinguishes between such artificial tissues.

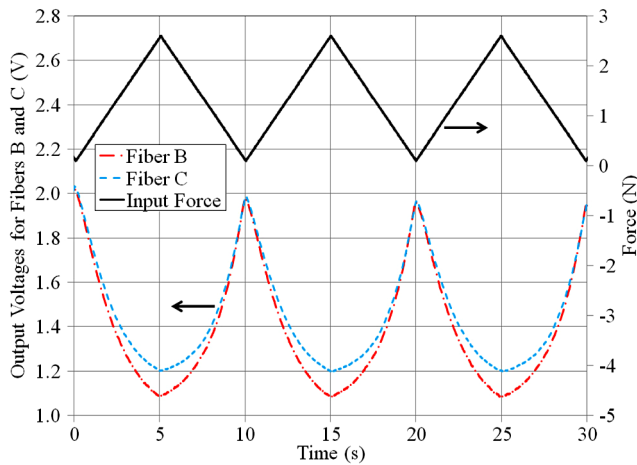


Fig. 10 Sensor output to detect the location of an embedded lump on the left part of the sensor inside the tissue.

annulus is the harder one, and the atrium has the moderate degree of softness. In terms of the linearity, Fiber A has a linear behavior, whereas Fibers B and C do not show linear behavior. However, in terms of hysteresis, the sensor output from all three Fibers A, B, and C show only a negligible amount. Even though the linearity and hysteresis of the sensor outputs have not been quantified, a qualitative analysis of these characteristics can be observed in Fig. 9.

In the second test, the ability of the sensor to detect the location of an embedded lump/artery was investigated. The conditions of the test are similar to Fig. 8(b) except that now a solid lump was embedded inside the artificial tissue in the left-half region of the sensor. A triangular waveform force with the amplitude between 0.1 and 2.5 N and with the frequency of 0.1 Hz was applied through the upper jaw of the test instrument. Figure 10 shows the sensor response to such test conditions from Fibers B and C. As can be seen, the output voltage of Fiber B is less than the output voltage of Fiber C. This means that the deformation of the left elastic foundation is more than the deformation of the right elastic foundation which confirms that the lump is located on the left-half region of the sensor beam.

In the last test, the capability of the sensor to perform under static loading conditions was examined. To do so, a square

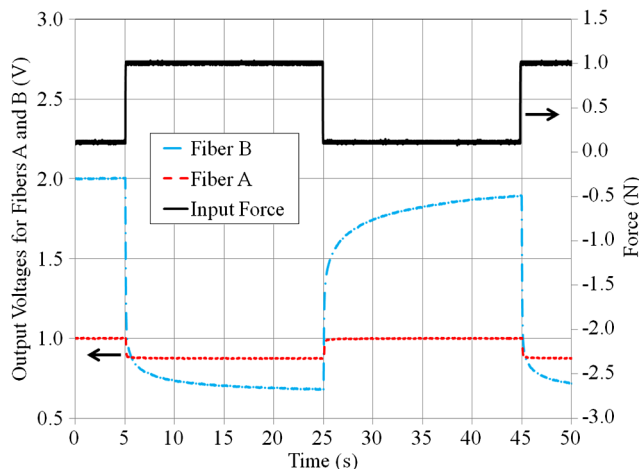


Fig. 11 Response of the sensor from Fibers A and (b) to a square input force function with the frequency of 0.025 Hz.

concentrated force function with the frequency of 0.025 Hz was applied on the sensor. Figure 11 shows the force applied to the sensor as well as the response of the sensor from Fibers A and B. Since Fiber B and Fiber C display similar behavioral patterns, only one of them, Fiber B, was considered in this test. Because Fiber A is attached to a rigid silicon structure, its output has negligible drift. However, Fiber B has more drift since it is indirectly attached to the elastic foundation. In fact, the time-dependent mechanical properties of PDMS elastic foundation (such as its relaxation and creep) result in the drift in the outputs of Fiber B and C. This drift can be minimized by changing the material of the elastic foundation to an elastic material with the minimum of viscoelastic properties.

7 Conclusions

This paper presents an innovative concept for an optical tactile sensor for diagnosing purposes during minimally invasive surgical tasks. The sensor measures the relative softness of tissues under both static and dynamic interactions. Moreover, the sensor diagnoses discontinuities in the softness along its sensing element. Such capability allows surgeons to distinguish between different types of tissues. More importantly, to address the needs of specific types of surgical tasks, the proposed sensor is MRI-compatible and also electrically passive. Using micro-systems technology, a prototype version of the sensor was micro-machined. To examine the sensor performance, a number of experimental tests were performed using soft objects as artificial tissues. Test results validate the sensor ability to measure the relative softness as well as the local discontinuities in the softness of tissues. In doing so, the sensor can be used to relatively distinguish various types of tissues during the interactions between surgical tools and tissues in surgical applications.

Acknowledgments

The authors would like to thank the Natural Sciences and Engineering Research Council of Canada (NSERC) and Concordia Research Chair for providing the financial support for the project.

References

1. G. T. Sung and I. S. Gill, "Robotic laparoscopic surgery: a comparison of the da Vinci and Zeus systems," *Urology* **58**(6), 893–898 (2001).
2. D. G. Jayne et al., "Robotic platforms for general and colorectal surgery," *Colorectal Disease* **13**(s7), 78–82 (2011).
3. B. Tang, S. Hou, and S. A. Cuschieri, "Ergonomics of and technologies for single-port laparoscopic surgery," *Minimally Invasive Therapy Allied Technol.* **21**(1), 46–54 (2012).
4. L. Di Biase et al., "Relationship between catheter forces, lesion characteristics, "popping," and char formation: Experience with robotic navigation system," *J. Cardiovasc. Electrophysiol.* **20**(4), 436–440 (2009).
5. Vanja Bozovic, *Medical Robotics*, I-Tech Education and Publishing, Vienna, Austria, 491–498 (2008).
6. C.-H. King et al., "Tactile feedback induces reduced grasping force in robot-assisted surgery," *IEEE Trans. Haptic* **2**(2), 103–110 (2009).
7. G. C. Burdea, *Force and Touch Feedback for Virtual Reality*, pp. 3–4, John Wiley & Sons, Inc., New York, NY (1996).
8. A. L. Trejos et al., "Robot-assisted tactile sensing for minimally invasive tumor localization," *Int. J. Robot. Res.* **28**(9), 1118–1133 (2009).
9. B. Kuebler et al., "Tactile feedback for artery detection in minimally invasive robotic surgery—preliminary results of a new approach," *Proc. IFMBE* **25**(6), 299–302 (2009).

10. K. Cleary et al., "Interventional robotic systems: applications and technology state-of-the-art," *Minim. Invasive Ther. Allied Technol.* **15**(2), 101–113 (2006).
11. K. Chinzei and K. Miller, "MRI guided surgical robot," in *Proc. 2001 Australian Conf. on Robotics and Automation*, pp. 50–55, Australian Robotics & Automation Association Inc. (ARAA), Sydney (2001).
12. K. Chinzei, R. Kikinis, and F. A. Jolesz, "MR compatibility of mechatronic devices: design criteria," in *Proc. 2nd Int. Conf. Med. Image Computing and Computer-Assisted Intervention*, pp. 1020–1031, Springer, Berlin Heidelberg (1999).
13. S. G. Yuen et al., "Robotic force stabilization for beating heart intracardiac surgery," in *Proc. 12th Int. Conf. Med. Image Computing and Computer-Assisted Intervention: part I*, pp. 26–33, Springer, Berlin Heidelberg (2009).
14. P. Puangmali et al., "State-of-the-art in force and tactile sensing for minimally invasive surgery," *IEEE Sens. J.* **8**(4), 371–381 (2008).
15. S. Schostek, M. O. Schurr, and G. F. Buess, "Review on aspects of artificial tactile feedback in laparoscopic surgery," *Med. Eng. Phys.* **31**(8), 887–898 (2009).
16. N. Zemiti et al., "Mechatronic design of a new robot for force control in minimally invasive surgery," *IEEE-ASME Trans. Mechatron.* **12**(2), 143–153 (2007).
17. J. Peirs et al., "A micro optical force sensor for force feedback during minimally invasive robotic surgery," *Sens. Actuator A-Phys.* **115**(2–3), 447–455 (2004).
18. S. Sokhanvar, M. Packirisamy, and J. Dargahi, "MEMS endoscopic tactile sensor: toward in-situ and in-vivo tissue softness characterization," *IEEE Sens. J.* **9**(12), 1679–1687 (2009).
19. S. Sokhanvar, M. Packirisamy, and J. Dargahi, "A multifunctional PVDF-based tactile sensor for minimally invasive surgery," *Smart Mater. Struct.* **16**(4), 989–998 (2007).
20. M. Kalantari et al., "A piezoresistive tactile sensor for tissue characterization during catheter-based cardiac surgery," *Int. J. Med. Robot. Comput. Assist. Surg.* **7**(4), 431–440 (2011).
21. M. Kalantari et al., "Design, fabrication, and testing of a piezoresistive hardness sensor in minimally invasive surgery," in *Proc. IEEE Haptics Symp.*, pp. 431–437, IEEE, Waltham, Massachusetts (2010).
22. J. A. C. Heijmans, L. K. Cheng, and F. P. Wieringa, "Optical fiber sensors for medical applications-practical engineering considerations," in *Proc. 4th European Conf. of the International Federation for Medical and Biological Engineering (IFMBE)*, pp. 2330–2334, Springer, Berlin Heidelberg (2008).
23. P. Polygerinos et al., "MRI-compatible fiber-optic force sensors for catheterization procedures," *IEEE Sens. J.* **10**(10), 1598–1608 (2010).
24. P. Puangmali et al., "Miniaturized triaxial optical fiber force sensor for MRI-guided minimally invasive surgery," in *Proc. 2010 IEEE International Conference on Robotics and Automation*, pp. 2592–2597, IEEE, Alaska (2010).
25. K. Yokoyama et al., "Novel contact force sensor incorporated in irrigated radiofrequency ablation catheter predicts lesion size and incidence of steam pop and thrombus," *Circ.-Arrhythmia Electrophysiol.* **1**(5), 354–362 (2008).
26. M. C. Yip, S. G. Yuen, and R. D. Howe, "A robust uniaxial force sensor for minimally invasive surgery," *IEEE Trans. Biomed. Eng.* **57**(5), 1008–1011 (2010).
27. R. Ahmadi et al., "Discretely-loaded beam-type optical fiber tactile sensor for tissue manipulation and palpation in minimally invasive robotic surgery," *IEEE Sens. J.* **12**(1), 22–32 (2012).
28. S. Nemoto and T. Makimoto, "Analysis of splice loss in single-mode fibres using a Gaussian field approximation," *Opt. Quant. Electron.* **11**(5), 447–457 (1979).
29. J. Li, Q. Zhang, and A. Liu, "Advanced fiber optical switches using deep RIE (DRIE) fabrication," *Sens. Actuator A-Phys.* **102**(3), 286–295 (2003).
30. F. P. Beer and E. R. Johnston, *Mechanics of Materials*, pp. 396–429, McGraw-Hill, New York (1981).